Monthly Notices
of the
ROYAL ASTRONOMICAL SOCIETY

Mon. Not. R. Astron. Soc. **401,** 2053–2058 (2010) doi:10.1111/j.1365-2966.2009.15793.x

Studies of dissipative standing shock waves around black holes

Santabrata Das,[1,2]★ Sandip K. Chakrabarti[3,4]★ and Soumen Mondal[1,5]★

[1]*Korea Astronomy and Space Science Institute, 61-1 Hwaam Dong, Yuseong-Gu, Daejeon 305 348, South Korea*
[2]*Indian Institute of Technology Guwahati, Guwahati, 781039 Assam, India*
[3]*S. N. Bose National Centre for Basic Sciences, JD-Block, Sector III, Salt Lake, Kolkata 700 098, India*
[4]*Centre for Space Physics, Chalantika 43, Garia Station Rd, Kolkata 700084, India*
[5]*Ramakrishana Mission Residential College, Narendrapur, Kolkata 103, India*

Accepted 2009 September 29. Received 2009 September 29; in original form 2009 March 11

ABSTRACT

We investigate the dynamical structure of advective accretion flow around stationary as well as rotating black holes. For a suitable choice of input parameters, such as accretion rate ($\dot{\mathcal{M}}$) and angular momentum (λ), a global accretion solution may include a shock wave. The post-shock flow is located at a few tens times the Schwarzchild radius and is generally very hot and dense. This successfully mimics the so-called Compton cloud, which is believed to be responsible for emitting hard radiation. Owing to the radiative loss, significant energy is removed from the accreting matter and the shock moves forward towards the black hole in order to maintain the pressure balance across it. We identify the effective area of parameter space ($\dot{\mathcal{M}}$–λ) that allows accretion flows to have some energy dissipation at the shock ($\Delta\mathcal{E}$). As the dissipation is increased, the parameter space is reduced and finally disappears when the dissipation reaches a critical value. The dissipation has a profound effect on the dynamics of post-shock flow. By moving forward, an unstable shock, the oscillation of which causes quasi-periodic oscillations (QPOs) in the emitted radiation, will produce oscillations of high frequency. Such an evolution of QPOs has been observed in several black hole candidates during their outbursts.

Key words: accretion, accretion discs – black hole physics – shock waves.

1 INTRODUCTION

In a significant work on the prospect of shock formation in an accretion disc around a black hole, Chakrabarti & Das (2004) showed that in order to have a stable shock, the viscous dissipation inside a flow must have an upper limit beyond which the Rankine–Hugoniot conditions cannot be satisfied. In Das & Chakrabarti (2004) and Das (2007), bremsstrahlung and synchrotron cooling were also added to dissipate away the heat generated from viscous dissipation. However, it is well known that the post-shock region emits hard X-rays in a black hole candidate (Chakrabarti & Titarchuk 1995), and some amount of energy is lost through radiation from the post-shock region. This radiative loss primarily comes from the thermal energy of the flow and takes place via thermal Comptonization. In a self-consistent shock condition, this radiative loss must also be incorporated. In the present paper, we quantitatively show how the energy loss at the shock affects the location of the shock itself around stationary as well as rotating black holes. As energy dissipation is increased the post-shock flow pressure is reduced, causing the shock front to come closer to the black hole in order to maintain the pressure balance across it. Accordingly, the dynamical properties of standing shock waves should be related directly to the amount of energy discharge from the post-shock flow. In addition, the mass outflow rate that is believed to be generated from the post-shock region (Chakrabarti 1999; Das et al. 2001b; Das & Chattopadhyay 2008) would also be affected by the energy discharge at the shock location. Therefore, it is pertinent to understand the response of energy dissipation with regard to the formation of standing shock waves. In this paper, we do precisely this.

The plan of our paper is as follows. In the next section, we present the equations governing the flow and the procedure we adopted to solve these equations. In Section 3, we show how the Rankine–Hugoniot conditions at the shocks must be modified when energy dissipation is present. In Section 4, we show the results of our computations. Finally, in Section 5, we present some concluding remarks.

2 GOVERNING EQUATIONS AND SONIC-POINT ANALYSIS

We start with a steady, thin, rotating, axisymmetric accretion flow around a black hole. We assume small accretion rates, so that the flow is radiatively inefficient and behaves essentially as a constant-energy flow, as in Chakrabarti (1989). We assume a polytropic

★E-mail: sbdas@canopus.cnu.ac.kr; sbdas@iitg.ernet.in (SD); chakraba@bose.res.in (SKC); soumen@bose.res.in (SM)

equation of state for the accreting matter, $P = K\rho^{\gamma}$, where P and ρ are the isotropic pressure and the matter density, respectively, γ is the adiabatic exponent, considered to be constant throughout the flow, and K is a constant that measures the entropy of the flow and can change only at the shock. Since we ignore viscous dissipation, the angular momentum of the flow $\lambda \equiv x\vartheta_{\theta}$ is also constant everywhere. However, we assume that the main dissipation is concentrated in the immediate vicinity of the post-shock flow, which would be the case if thermal Comptonization were the dominant process. The flow height is determined from the condition of being in equilibrium in a direction perpendicular to the equatorial plane. Flow equations are made dimensionless by considering units of length, time and mass as $GM_{\rm BH}/c^2, GM_{\rm BH}/c^3$ and $M_{\rm BH}$ respectively, where G is the gravitational constant, $M_{\rm BH}$ is the mass of the black hole and c is the velocity of light.

In the steady state, the dimensionless energy equation at the disc equatorial plane is given by (Chakrabarti 1989)

$$\mathcal{E} = \frac{1}{2}\vartheta^2 + \frac{a^2}{\gamma - 1} + \Phi, \tag{1}$$

where $\mathcal{E}$ is the specific energy, ϑ the radial velocity and a the adiabatic sound speed, defined as $a = \sqrt{\gamma P/\rho}$. Here, the effective potential due to the black hole is denoted by Φ. In the present study, the effect of gravity is taken care of by two different potentials. To represent a Schwarzschild black hole we use the Paczyński–Wiita (Paczynski & Wiita 1980) potential ($\Phi_{\rm PW}$), and for a Kerr black hole we consider the pseudo-Kerr potential ($\Phi_{\rm PK}$) introduced by Chakrabarti & Mondal (2006). It has been adequately shown that these potentials accurately mimic not only the geometry of the space–time, but also the dynamics of the flow. In fact the error arising from not using a full general relativistic treatment has been shown to be at the most a few per cent (Chakrabarti & Mondal 2006). The expressions for Paczyński–Wiita and pseudo-Kerr effective potentials are respectively given by

$$\Phi_{\rm PW} = \frac{\lambda^2}{2x^2} - \frac{1}{2(R-1)}$$

and

$$\Phi_{\rm PK} = -\frac{B + \sqrt{B^2 - 4AC}}{2A},$$

where

$$A = \frac{\alpha^2\lambda^2}{2x^2},$$

$$B = -1 + \frac{\alpha^2\omega\lambda R^2}{x^2} + \frac{2a_k\lambda}{R^2 x},$$

$$C = 1 - \frac{1}{R - x_0} + \frac{2a_k\omega}{x} + \frac{\alpha^2\omega^2 R^4}{2x^2}.$$

Here, x and R represent the cylindrical and spherical radial distance from the black hole when the black hole itself is considered to be located at the origin of the coordinate system. Here, $x_0 = (0.04 + 0.97a_k + 0.085a_k^2)/2, \omega = 2a_k/(x^3 + a_k^2 x + 2a_k^2)$ and $\alpha^2 = (x^2 - 2x + a_k^2)/(x^2 + a_k^2 + 2a_k^2/x)$, where α is the redshift factor and a_k represents the black hole rotation parameter, defined as the specific spin angular momentum of the black hole.

The mass-flux conservation equation in the steady state, apart from a geometric factor, is given by

$$\dot{M} = \vartheta\rho x h(x), \tag{2}$$

where $\dot{M}$ is the mass accretion rate, considered to be constant, and $h(x)$ represents the half-thickness of the flow (Chakrabarti 1989), which is expressed as

$$h(x) = a\sqrt{\frac{x}{\gamma\Phi_R^{'}}}. \tag{3}$$

Here, $\Phi_R^{'} = (\partial\Phi/\partial R)_{z\ll x}$ and z is the vertical height in the cylindrical coordinate system where $R = \sqrt{x^2 + z^2}$. By using the polytropic equation of state and the definition of the adiabatic sound speed, we obtain the equation for the so-called 'entropy accretion rate' (Chakrabarti 1989) as

$$\dot{\mathcal{M}} = \vartheta a^{\nu}\sqrt{\frac{x^3}{\gamma\Phi_R^{'}}}, \tag{4}$$

where $\nu = (\gamma + 1)/(\gamma - 1)$.

In order to form shocks, an accretion flow must be supersonic at some point, i.e. stationary flow must pass through a sonic point. We derive the sonic-point conditions following the standard sonic-point analysis (Chakrabarti 1989). We therefore differentiate equations (1) and (4) with respect to x and eliminate terms that involve derivatives of a to obtain the radial velocity gradient, which is expressed as

$$\frac{{\rm d}\vartheta}{{\rm d}x} = \frac{N}{D}, \tag{5}$$

where the numerator N and the denominator D are respectively given by

$$N = \frac{3a^2}{x(\gamma + 1)} - \frac{{\rm d}\Phi_{\rm e}}{{\rm d}x} - \frac{a^2}{(\gamma + 1)\Phi_R^{'}}\frac{{\rm d}\Phi_R^{'}}{{\rm d}x} \tag{5a}$$

and

$$D = \vartheta - \frac{2a^2}{(\gamma + 1)\vartheta}. \tag{5b}$$

Here, a subscript 'e' signifies that a quantity was calculated on the equatorial plane.

In order to have the flow smooth everywhere, the numerator and the denominator in equation (5) must vanish simultaneously. These considerations allow us to obtain the sonic-point conditions. Therefore, setting $D = 0$, we have

$$\vartheta_{\rm c}^2(x_{\rm c}) = \frac{2}{(\gamma + 1)}a_{\rm c}^2(x_{\rm c}) \;\Rightarrow\; M_{\rm c} = \sqrt{\frac{2}{\gamma + 1}}. \tag{6a}$$

The subscript 'c' signifies that the quantity was computed at the sonic points. Note that the Mach number $[M(x_{\rm c})]$ at the sonic point is not unity as in the other models, since the vertical equilibrium model is considered. The other condition arises while setting $N = 0$, and is given by

$$a_{\rm c}^2(x_{\rm c}) = (\gamma + 1)\left(\frac{{\rm d}\Phi_{\rm e}}{{\rm d}x}\right)_{\rm c}\left[\frac{3}{x} - \frac{1}{\Phi_R^{'}}\frac{{\rm d}\Phi_R^{'}}{{\rm d}x}\right]_{\rm c}^{-1}. \tag{6b}$$

The sound speed at the sonic point can now easily be calculated from equation (6b) and must be always positive. The flow may possess at most three sonic points outside the black hole horizon. Among them, the closest one to the black hole is called the inner sonic point whereas the furthest one is known as the outer sonic point. The nature of the sonic point solely depends on the value of the velocity gradient (equation 5) at the sonic point. Usually, ${\rm d}\vartheta/{\rm d}x$ has two values at the sonic point: one is for accretion flow and the other is for winds. A sonic point is referred to as 'saddle-type' when both the derivatives are real and of opposite sign. When the derivatives

are real and of the same sign, the sonic point is called a 'nodal-type'. If the derivatives are complex, the sonic point is 'centre-type'. The saddle-type sonic point has special importance, as transonic flow can only pass through it. Moreover, for standing shock transition, a flow must have multiple saddle-type sonic points. We solve equations (1)–(6) to obtain a full set of global flow solutions where a standing shock may be present.

3 SHOCK CONDITIONS AND SHOCK INVARIANT

In order to have a shock, the flow velocity must jump discontinuously from the supersonic to the subsonic branch. This discontinuous shock jump is characterized by four flow variables, namely shock location (x_s), radial velocity (ϑ), sound speed (a) and entropy constant (K). These are given respectively by

$$x = x_s, \tag{7a}$$

$$\Delta\vartheta = \vartheta_+(x_s) - \vartheta_-(x_s), \tag{7b}$$

$$\Delta a = a_+(x_s) - a_-(x_s) \tag{7c}$$

and

$$\Delta K = K_+ - K_-, \tag{7d}$$

where the subscripts '−' and '+' denote the quantities before and after the shock. Here, we are dealing with a quasi-two-dimensional flow where pressure and density are averaged over the vertical direction. In this case, the Rankine–Hugoniot shock conditions (Landau & Lifshitz 1959) are given by

$$\mathcal{E}_+ = \mathcal{E}_- - \Delta\mathcal{E}, \tag{8a}$$

(II) the self-consistent pressure condition,

$$W_+ + \Sigma_+\vartheta_+^2 = W_- + \Sigma_-\vartheta_-^2, \tag{8b}$$

and (III) the baryon number conservation equation,

$$\dot{M}_+ = \dot{M}_-. \tag{8c}$$

Here, W and Σ denote the vertically averaged pressure and density of the flow (Matsumoto et al. 1984).

Because of our choice of radiatively inefficient flow, i.e. flow with low accretion rates, the energies $\mathcal{E}_-$ and $\mathcal{E}_+$ are nearly constant. However, in the presence of dissipation at the shock, $\Delta\mathcal{E}$ will be non-zero. Since the dissipation is expected to be mostly through thermal Comptonization, which may cool the flow from ∼100 keV to ∼3 keV (Chakrabarti & Titarchuk 1995), we assume that the energy dissipation in the post-shock region reduces the temperature of the flow and the loss of energy is proportional to the temperature difference between the post-shock and pre-shock flows, similarly to the well-known Kirchoff's law, i.e.

$$\Delta\mathcal{E} = \Delta\mathcal{E}'(a_+^2 - a_-^2),$$

where $\Delta\mathcal{E}'$ is the proportionality constant, which will be used as a parameter. In reality, this is a function of the electron and low-energy photon contents of the accretion flow and can be calculated in any situation (Chakrabarti & Titarchuk 1995). Since the thermal energy content (the final term in equation 1) can be anywhere between 10–30 per cent of the rest-mass energy, a few per cent of thermal energy can be easily extracted. Below, we show that the maximum dissipation for a black hole of $a \sim 0.8$ is about 6.5 per cent.

(I) the energy conservation equation.

Using the governing equations and shock conditions, we compute an invariant relation at the shock (Chakrabarti 1990), which is given by

$$\begin{aligned} C &= \frac{[M_+(3\gamma-1)+(2/M_+)]^2}{2+(\gamma-1)M_+^2+2(\gamma-1)\Delta\mathcal{E}'} \\ &= \frac{[M_-(3\gamma-1)+(2/M_-)]^2}{2+(\gamma-1)M_-^2+2(\gamma-1)\Delta\mathcal{E}'}, \end{aligned} \tag{9}$$

where $M_\pm$ denote the Mach numbers of the flow.

Simplifying equation (9), we have the following relations:

$$M_\pm = \frac{-\mathcal{Y} \pm \sqrt{\mathcal{Y}^2 - 4\mathcal{X}\mathcal{Z}}}{2\mathcal{X}} \tag{10}$$

and

$$M_+M_- = \frac{2}{\sqrt{(3\gamma-1)^2 - C(\gamma-1)}}, \tag{11}$$

where

$\mathcal{X} = (3\gamma-1)^2 - C(\gamma-1)$,

$\mathcal{Y} = 2\left[2(3\gamma-1) - C - C(\gamma-1)\Delta\mathcal{E}'\right]$ and

$\mathcal{Z} = 4$.

The flow will pass through the shock if the shock-invariant condition is satisfied (equation 9) at some point between the two saddle-type sonic points.

4 RESULTS

Fig. 1 shows a phase-space trajectory of accretion flow around a Schwarzschild black hole where the logarithmic radial distance is plotted along the horizontal axis and the Mach number

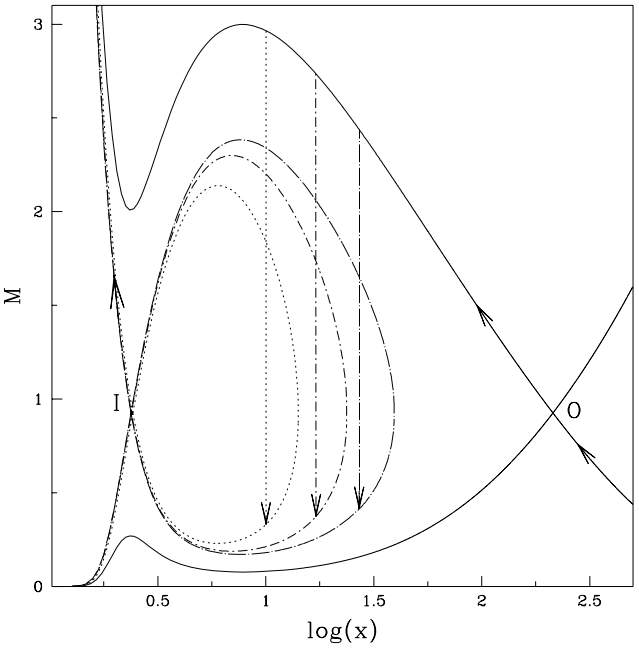

Figure 1. Phase-space diagram of accretion flow in the $M-\log x$) plane. Flow parameters are $\lambda = 3.56$ and $\mathcal{M} = 0.08 \times 10^{-5}$. The energy at the outer sonic point is obtained as $\mathcal{E} = 0.13452 \times 10^{-2}$. The vertical lines indicate the possible shock transitions $x_s = 27.75$ (long-dash–dotted), $x_s = 17.02$ (short-dash–dotted) and $x_s = 10.001$ (dotted) corresponding to energy dissipation at the shock $\Delta\mathcal{E} = 0.699 \times 10^{-3}$, 0.37×10^{-2} and 0.985×10^{-2} respectively. Shocks form closer to the black hole horizon as the energy dissipation at the shock is enhanced.

($M = \vartheta/a$) is plotted along the vertical axis. Arrows indicate the direction of the accreting flow. Here, the flow parameters are $\lambda = 3.56$, $\dot{\mathcal{M}} = 0.08 \times 10^{-5}$ and $\gamma = 4/3$. Subsonic accreting flow passes through the outer sonic point (O) and becomes supersonic. Depending on the energy dissipation at the shock ($\Delta\mathcal{E}$), shock conditions are satisfied at some particular location and the flow makes a discontinuous jump (shock transition) from the supersonic branch to the subsonic branch there. After the shock transition, the flow momentarily slows down and subsequently picks up its velocity to cross the inner sonic point (I) before entering into the black hole. Since the flow loses a part of its energy at the shock in the form of thermal energy, the pressure in the post-shock region is diminished. As a result, the shock moves forward to maintain a pressure balance across it. The possible shock transitions at x_s are shown as vertical lines for various energy dissipations at the shock. For a given set of input parameters ($\lambda = 3.56$, $\dot{\mathcal{M}} = 0.08 \times 10^{-5}$), the shock forms closer to the black hole horizon as the energy dissipation at the shock increases. For instance, $x_s = 27.75$, $\Delta\mathcal{E} = 0.699 \times 10^{-3}$ (long-dash–dotted), $x_s = 17.02$, $\Delta\mathcal{E} = 0.37 \times 10^{-2}$ (short-dash–dotted) and $x_s = 10.0$, $\Delta\mathcal{E} = 0.985 \times 10^{-2}$ (dotted) respectively.

In Fig. 2, we present the variation of shock location on a logarithmic scale as a function of the energy dissipation at the shock. In the upper panel, we show the results obtained by using the Paczyński–Wiita potential while in the lower panel we use the pseudo-Kerr potential. In Fig. 2(a), the accretion rate is chosen as $\dot{\mathcal{M}} = 0.01 \times 10^{-5}$ and the adiabatic index is $\gamma = 4/3$. Different curves are drawn for a set of angular momenta starting from $\lambda = 3.46$ (leftmost curve) to $\lambda = 3.82$ (rightmost curve) with an interval of d $\lambda = 0.04$. In Fig. 2(b), we consider $\dot{\mathcal{M}} = 0.01 \times 10^{-6}$ and black hole rotation parameter $a_k = 0.5$. In this plot, the angular momentum is varied from $\lambda = 3.14$ (leftmost curve) to $\lambda = 3.30$ (rightmost curve) with an interval of d $\lambda = 0.04$. Both panels indicate that the shock forms closer to the black hole horizon as the energy dissipation increases monotonically for given input parameters ($\dot{\mathcal{M}}$, λ). This conclusion is valid for both rotating and non-rotating black holes. Note that there is a cut-off for each individual curve. At very high energy dissipation, Rankine–Hugoniot shock conditions (RHC) are not satisfied and no steady shocks can form. However, non-steady shocks may still form as accreting matter continues to possess multiple sonic points where entropy at the inner sonic point is higher than at the outer sonic point (Das, Chattopadhyay & Chakrabarti 2001a). In this case, the shock location becomes imaginary and the shock starts oscillating with a time period that is comparable to the inverse of the observed quasi-periodic oscillation (QPO) frequencies of black hole candidates. In order to investigate this physical process explicitly a rigorous time-dependent analysis is required, which is beyond the scope of our present work. As the angular momentum is increased, the maximum energy dissipation at the shock first increases, becomes a maximum at some λ and then decreases. For a non-rotating black hole, the maximum energy dissipation at the shock ($\Delta\mathcal{E}_{\rm max}$) is around 3.5 per cent for accretion flows with angular momentum $\lambda = 3.70$, and for a rotating black hole $\Delta\mathcal{E}_{\rm max}$ is around 4.7 per cent for $\lambda = 3.22$.

A diagram similar to Fig. 2 is drawn in Fig. 3 for various entropy accretion rates, keeping the specific angular momentum fixed. In the upper panel, we present the results for flows with angular momentum $\lambda = 3.70$ accreting on to a non-rotating black hole. Here, $\dot{\mathcal{M}}$ is varied from $\dot{\mathcal{M}} = 0.01 \times 10^{-5}$ (leftmost) to 0.21×10^{-5} (rightmost) with an interval of d$\dot{\mathcal{M}} = 0.01 \times 10^{-5}$. In the lower panel, we present a similar plot for flows of angular momentum $\lambda = 3.22$ accreting around a rotating black hole with rotation parameter $a_k = 0.5$. The accretion rate is chosen to be $\dot{\mathcal{M}} = 0.01 \times 10^{-6}$ (leftmost curve) to 0.16×10^{-6} (rightmost curve) with an interval of d$\dot{\mathcal{M}} = 0.05 \times 10^{-6}$. In both the panels, for a given accretion rate the shock front moves forward with the enhancement of energy dissipation at the shock. Interestingly, there is a significant reduction in maximum energy dissipation ($\Delta\mathcal{E}_{\rm max}$) at the shock as $\mathcal{M}$ is increased. Thus the parameter space for standing shocks is reduced with the increase of energy dissipation at the shock.

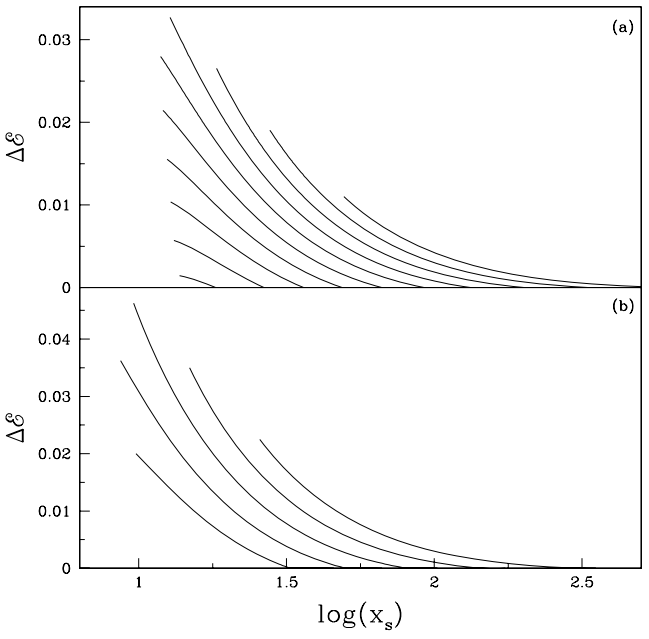

Figure 2. Variation of the energy dissipation at the shock as a function of shock location. (a) The accretion rate of the flow is chosen as $\dot{\mathcal{M}} = 0.01 \times 10^{-5}$. Curves are plotted for a set of angular momenta starting from $\lambda = 3.46$ (leftmost curve) to $\lambda = 3.82$ (rightmost curve) with an interval of d $\lambda = 0.04$. (b) The accretion rate of the flow is chosen as $\dot{\mathcal{M}} = 0.01 \times 10^{-6}$. The leftmost curve is drawn for $\lambda = 3.14$ and other curves are for increasing angular momentum with an interval of d $\lambda = 0.04$.

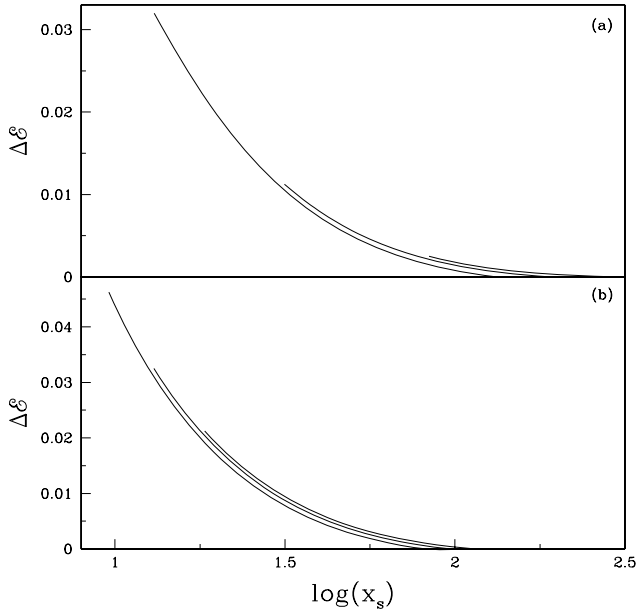

Figure 3. Plot of the energy dissipation at the shock as a function of shock location for a given angular momentum. (a) $\lambda = 3.70$ and (b) $\lambda = 3.22$. See text for more details.

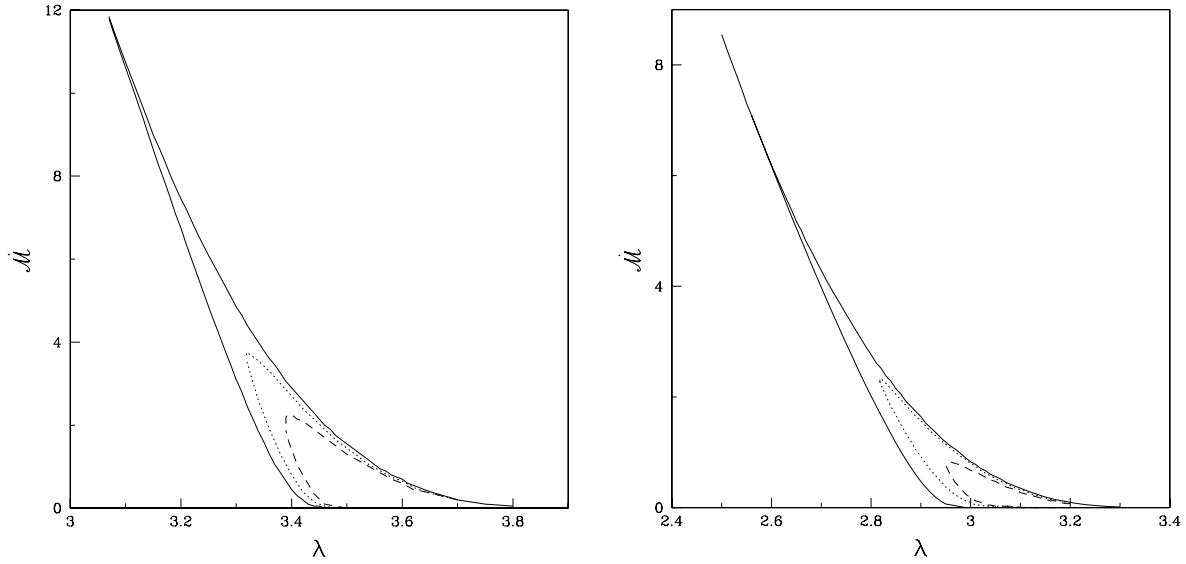

Figure 4. Modification of the region of parameter space that forms a standing shock as a function of energy dissipation ($\Delta\mathcal{E}$) at the shock. Left panel: non-rotating black hole; right panel: rotating black hole ($a_k = 0.5$). The parameter space shrinks with the increase of $\Delta\mathcal{E}$.

In Fig. 4, we classify the parameter space spanned by the accretion rate ($\dot{\mathcal{M}}$) and the angular momentum (λ) in the region that allows standing shocks for various values of energy dissipation at the shock. In the left and right panels, the parameter spaces are obtained for non-rotating and rotating black holes. Here, the rotating black hole has $a_k = 0.5$. In the left panel, the parameter space under the solid curve is obtained for a dissipation-free accretion flow. The regions under the dotted and dashed curves are obtained for $\Delta\mathcal{E} = 1.5 \times 10^{-3}$ and 3.0×10^{-3} respectively. Similarly, in the right panel, the parameter spaces separated by solid, dotted and dashed curves are obtained for $\Delta\mathcal{E} = 0.0,\ 1.0 \times 10^{-3}$ and 4.0×10^{-3}. These figures show that the effective region of parameter space shrinks with the increase of energy dissipation at the shock on the lower angular momentum side. Above a critical limit of $\Delta\mathcal{E}$, this region disappears completely.

An important part of understanding an accretion flow around a rotating black hole is to compute the maximum energy dissipation ($\Delta\mathcal{E}_{\rm max}$) at the shock as a function of the black hole rotation parameter a_k. In Fig. 5, we present the variation of $\Delta\mathcal{E}_{\rm max}$ with a_k. For instance, for a weakly rotating black hole $\Delta\mathcal{E}_{\rm max}$ is around 2.5 per cent. For increasing a_k, $\Delta\mathcal{E}_{\rm max}$ increases and it reaches up to 6.5 per cent for a rapidly rotating black hole. However, the maximum available energy is around 5.7 per cent and 13 per cent of the rest-mass energy for $a_k = 0$ and $a_k = 0.8$ respectively. Thus we find that the maximum released energy at the shock is about 40–50 per cent of the available energy.

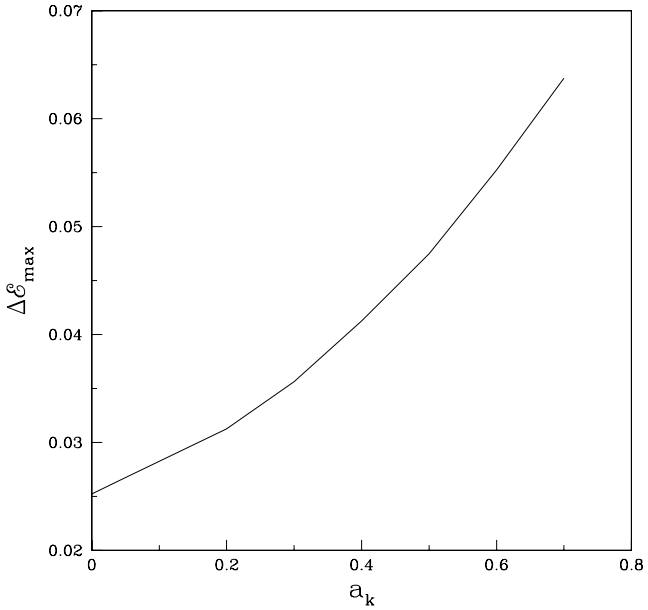

Figure 5. Variation of $\Delta\mathcal{E}_{\rm max}$ with black hole rotation parameter a_k. See text for more details.

5 CONCLUSIONS

It is well known that accretion flows around a stellar-mass black hole emit hard X-rays from a Compton cloud located close to the inner edge of the disc (Chakrabarti & Titarchuk 1995). This Compton cloud is the post-shock region, which also produces jets and outflows from the disc. The Comptonization process removes mainly the thermal energy of the flow. In this paper, we show that at a standing shock the maximum release of energy could be as high as 40–50 per cent of the maximum available energy. Since radiative loss removes significant thermal pressure from the inflow, the location of the shock is affected. In particular, the shock seems to form closer to the black hole when the dissipation is increased, due to the drop of the post-shock pressure, which can no longer support the shock in its original place. The implication of this could be profound. First of all, the observed QPOs are considered to be due to the oscillation of this shock. During outbursts, the QPOs of several black hole candidates, such as XTE J1550−564 and GRO J1655−40, evolve rapidly. The frequency changes from several mHz to a few tens of Hz in the rising phase of the outbursts. Since the QPO frequency is inversely proportional to the infall time of the post-shock flow, such evolution indicates that the shocks actually propagate towards the black hole during the rising phase of the outbursts (Chakrabarti et al. 2008; Chakrabarti, Datta & Pal 2009). Our mechanism discussed here gives a plausible explanation for such a phenomenon.

ACKNOWLEDGMENTS

SKC's work is partly supported by a RESPOND project and SD is partly supported via a postdoctoral fellowship from the Korea Astronomy and Space Science Institute (KASI).

REFERENCES

Chakrabarti S. K., 1989, ApJ, 347, 365
Chakrabarti S. K., 1990, Theory of Transonic Astrophysical Flows. World Scientific Publishing, Singapore
Chakrabarti S. K., 1999, A&A, 351, 185
Chakrabarti S. K., Das S., 2004, MNRAS, 349, 649
Chakrabarti S. K., Mondal S., 2006, MNRAS, 369, 976
Chakrabarti S. K., Titarchuk L. G., 1995, ApJ, 455, 623
Chakrabarti S. K. Debnath D., Nandi A., Pal P. S., 2008, A&A, 489, 41
Chakrabarti S. K., Datta B. G., Pal P. S., 2009, MNRAS, 394, 1463
Das S., 2007, MNRAS, 376, 1659
Das S., Chakrabarti S. K., 2004, Int. J. Mod. Phys. D, 13, 1955
Das S., Chattopadhyay I., 2008, New Astron., 13, 549
Das S., Chattopadhyay I., Chakrabarti S. K., 2001a, ApJ, 557, 983
Das S., Chattopadhyay I., Nandi, A., Chakrabarti S. K., 2001b, A&A, 379, 683
Landau L. D., Lifshitz E. D., 1959, Fluid Mechanics. Pergamon Press, New York
Matsumoto R., Kato S., Fukue J., Okazaki A. T., 1984, PASJ, 36, 7
Paczynski B., Wiita P. J., 1980, A&A, 88, 23

This paper has been typeset from a TEX/LATEX file prepared by the author.